American Mineralogist, Volume 97, pages 291–298, 2012

Combined neutron and X-ray diffraction determination of disorder in doped zirconolite-2*M*

Karl R. Whittle,[1,2,*] Neil C. Hyatt,[2] Katherine L. Smith,[1] Irene Margiolaki,[3] Frank J. Berry,[4,†] Kevin S. Knight,[5] and Gregory R. Lumpkin[1]

[1]Institute of Materials and Engineering Science, Australian Nuclear Science and Technology Organisation, Locked Bag 2001, Kirrawee DC, New South Wales 2232, Australia
[2]Department of Materials Science and Engineering, University of Sheffield, Mappin Street, Sheffield S1 3JD, U.K.
[3]European Synchrotron Radiation Facility, 6 rue Jules Horowitz, BP220, 38043, Grenoble Cedex, France
[4]Department of Chemistry, The Open University, Walton Hall, Milton Keynes, Bucks MK7 6AA, U.K.
[5]ISIS Facility, Rutherford Appleton Laboratory, Chilton, Didcot, Oxfordshire OX11 0QX, U.K.

Abstract

Zirconolites based on the replacement of Ti^{4+} with equimolar amounts of $Nb^{5+}$and Fe^{3+}, $CaZrTi_{2-2x}Nb_xFe_xO_7$, have been jointly refined using high-resolution neutron powder diffraction and resonant X-ray powder diffraction data, with extra information provided from ^{57}Fe Mössbauer spectroscopy, to determine cation disorder. The results indicate that the $CaZrTi_{2-2x}Nb_xFe_xO_7$ series adopts the zirconolite-2*M* polytype across the range, with the replacement of Ti^{4+} by Fe^{3+} and Nb^{5+} located within the hexagonal tungsten bronze (HTB) layers. Mössbauer spectroscopy shows that Fe^{3+} preferentially fills the Ti split (C2) site, with secondary filling of the C1 site and no observable occupancy of the C3 site. This has been confirmed by neutron and resonant X-ray diffraction. Niobium has been found to occupy both the C1 and C3 sites with no evidence for occupancy of the C2 site.

Keywords: Zirconolite, resonant X-ray diffraction, neutron diffraction, Mössbauer

Introduction

Zirconolites (Berry et al. 2005; Ewing 2007; Lumpkin 2001; Yudintsev 2003), based on $CaZrTi_2O_7$, are an important class of accessory mineral that can accommodate a wide range of cations. Natural zirconolite varies extensively, with lanthanides (Ln), actinides (Act), Nb, and Fe found to be the main impurities. The zirconolite structure-type has been proposed as a mechanism by which highly radioactive actinide waste can be immobilized, predominantly due to this ability. In natural samples, lanthanides and actinides often replace Ca^{2+}cations, with overall charge balance being maintained by partial replacement of Ti^{4+} by lower charged cations, such as Al^{3+}, Mg^{2+}, and Fe^{3+}.

The zirconolite structure, a derivative of pyrochlore, is formed from a contraction perpendicular to one of the pyrochlore (111) planes. This contraction gives rise to a layered structure consisting of alternating hexagonal tungsten bronze (HTB) and Ca/Zr layers parallel to (001), which is found to adopt monoclinic symmetry (*C*2/*c*), example images are shown in Figure 1. When compared to pyrochlore ($A_2B_2O_7$) the cations are more ordered, giving a general formula of ABC_2X_7, where A = Ca^{2+}, Ln^{3+}, Act; B = Zr^{4+}, Hf^{4+}, Ln^{3+}, Act; and C = Ti^{4+}, Zr^{4+}, Nb^{5+}, Fe^{3+}, Mg^{2+}, Al^{3+}, W^{6+}, and other minor elements. The C cation adopts three distinct sites, two octahedral sites (C1 and C3) describing the HTB motif and an unusual, split site lying within the six membered ring (C2) offset from the middle. This latter site replaces one of the A site cation positions in the parent pyrochlore structure. Several polytypes are possible in zirconolite, depending on how the HTB and Ca/Zr layers are stacked. In addition to monoclinic 2*M* (*C*2/*c*) zirconolite studied here, hexagonal (Grey et al. 2003) 3*T* and monoclinic (Coelho et al. 1997) 4*M* (*C*2/*c*) are examples of further polytypes that have been identified.

Previously the cation distribution has been studied (Berry et al. 2005; Lumpkin et al. 2006) by continuous replacement of Ti^{4+} by Fe^{3+} and Nb^{5+}, in the manner $CaZrTi_{2-2x}Fe_xNb_xO_7$ where x = 0 to 1 in steps of 0.1 using single wavelength synchrotron X-ray powder diffraction and ^{57}Fe Mössbauer spectroscopy. In this work, the cation distribution is investigated using a coupled Rietveld refinement of neutron and resonant X-ray diffraction data combined with the extra information about Fe^{3+} location ^{57}Fe Mössbauer spectroscopy provides.

Experimental methods

Sample preparation

The samples used were those previously studied by Lumpkin et al. (2006), a summary of preparation is presented here, for further discussion about sample purity see that study.

Samples of composition $CaZrTi_{2-2x}Nb_xFe_xO_7$, x = 0.1, 0.2...1.0, were prepared from $Ca(NO_3)_3{\cdot}4H_2O$ (Aldrich, 99%), $Fe(NO_3)_3{\cdot}9H_2O$ (Aldrich, 99.5%), Nb_2O_5 (Aldrich, 99.9%), $Zr[OCH(CH_3)_2]_4{\cdot}(CH_3)_2CHOH$ (Aldrich, 99.9%) and $Ti[OCH(CH_3)_2]_4$ (Aldrich, 99%, characterized for Ti content) precursors. Stoichiometric amounts of nitrate precursor were dissolved in a large excess of water, to which Nb_2O_5 was added and thoroughly mixed until fully dispersed. The required volume of Zr and Ti precursor were added to ethanol, and the resultant solution was precipitated out through addition to the nitrate/oxide solution. This "flocculent" mixture was homogenized to ensure complete mixing, and dried on a hot plate. After drying the mixture was ground and calcined in an aluminum crucible at 750 °C in air for 1 h. These fired powders were ground to a fine powder by ball milling for 16 h with Y-stabilized ZrO_2 milling media, in H_2O. The final samples were sintered as pellets at 1400 °C for 20 h.

* E-mail: karl.whittle@ansto.gov.au
† Present address: School of Chemistry, University of Birmingham, Edgbaston, Birmingham B15 2TT, U.K.

0003-004X/12/0203–291$05.00/DOI: http://dx.doi.org/10.2138/am.2012.3848

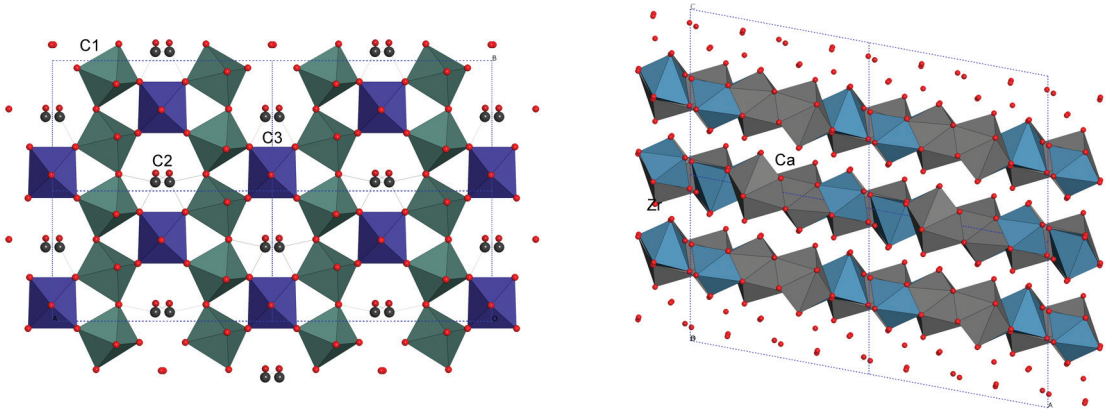

FIGURE 1. Unit-cell representations of zirconolite-2*M*, with the cation crystal sites labeled. The image on the left shows the hexagonal tungsten bronze (HTB) layer arising from the C2, C2, and C3 cations, with the C1 and C3 cations showed as octahedra, viewed down the (001) direction. The C2 cation is shown as bonded atoms, indicating the close nature of the two sites which precludes both sites being occupied simultaneously. The image on the right shows the Ca and Zr polyhedral layers, which alternate with the HTB layers (omitted for clarity), viewed down the (010) direction.

Mössbauer spectroscopy

^{57}Fe Mössbauer spectra, for samples x = 0.2, 0.4, 0.6, 0.8, and 1.0, were recorded at 298 K using a microprocessor controlled spectrometer with a ca. 25 mCi ^{57}Co/Rh source. All spectra were computer fitted and the chemical isomer shift data are quoted relative to that of metallic iron at 298 K.

High-resolution neutron diffraction

Time-of-flight powder neutron diffraction data for x = 0, 0.2, 0.3, 0.5, 0.7, 0.9 and 1.0, were collected using the HRPD diffractometer at the U.K. pulsed spallation neutron source ISIS, Rutherford Appleton Laboratory (Ibberson et al. 1992), during November 2004. For each composition studied, between 1 and 10 g of powdered sample was loaded into a thin-walled, cylindrical vanadium sample can and diffraction data collected for between 500 and 1500 μAh of integrated beam current, dependent on sample quantity. Summed and normalized data collected in the two available detectors located at 90° and 168° incident to the incoming flux over the time-of-flight range ~50 to 130 ms (corresponding to a *d*-spacing range of ~1 to 3.2 Å, and 0.8 to 3.2 Å, respectively) were analyzed.

Resonant X-ray diffraction

High-resolution X-ray diffraction data were collected using the ID31 powder diffractometer at the European Synchrotron Radiation Facility (Fitch 2004). Data were collected at the following energies:

• Zr *K*-edge: 17.912, 17.990, and 18.015 keV, corresponding to the wavelengths 0.6921, 0.6892, and 0.6882 Å, respectively.

• Nb *K*-edge 18.988 and 19.002 keV corresponding to the wavelengths 0.65290 and 0.6520 Å. A third measurement at 18.977 keV (0.6533 Å) was undertaken but due to absorption from the inclusive Zr component the resultant data were poor, noisy, and unreliable. As a result it was not included in the refinements.

The changes in both f' and f'' were determined via a Kramers-Kronig transformation of measured sample absorption across the Zr and Nb *K*-edges. The exact wavelengths, and thus the correct f' and f'' for the elements under investigation, were determined using a silicon standard (NBS640c) to determine one wavelength for each elemental edge, and then use this wavelength to determine unit-cell size. Since unit-cell sizes do not change as a function of wavelength, this was subsequently used to determine the wavelength of measurement. The f' and f'' values for the remaining elements were calculated using f-prime (Larson and Von Dreele 1994) for the wavelength being used.

Rietveld refinements

The neutron and resonant X-ray diffraction data were refined using combined multiple refinements using GSAS with the EXPGUI toolkit (Larson and Von Dreele 1994; Toby 2001). The data sets were initially refined individually, using a Le Bail type refinement (Le Bail et al. 1988), to obtain initial parameters for background, based on a Chebyschev polynomial background function and peak shape, based on a mixed Gaussian-Lorenztian for the X-ray data and time of flight for the neutron diffraction data. The data were subsequently analyzed in a coupled refinement with all sets of data refining unit-cell parameters (biased to the X-ray measurements due to the inherent higher resolution), atomic positions, isotropic thermal parameters, and cation disorder.

RESULTS

Mössbauer spectroscopy

The ^{57}Fe spectra were fitted using two quadrupolar doublets, the values of which are shown in Table 1, and an example least-squares refinement is shown in Figure 2. The doublet showing the larger quadrupolar splitting, and thus a heavily distorted environment has been assigned to the split C2 site. This crystallographic site is composed of two TiO_4 tetrahedra sharing a common edge, with an inter-site distance of ~0.7 Å, coupled with a 50% occupancy, i.e., it is not possible for both sites to be occupied at the same time, see Figure 1. Thus when the cation is located on this site it can be bonded to 5 O^{2-} cations, average bond lengths 1.85–2.4 Å, giving rise to a large asymmetric electric field gradient and thus a large quadrupolar splitting. The values obtained from the fitting are close to those found for a spilt site in $SrFe_{12}O_{19}$ with similar geometry, providing a secondary confirmation for site assignment (Berry et al. 2001).

The second of the two doublets proved more difficult to assign within the structure. As it provides extra information about the location and proportion of Fe^{3+}, it is vital in the structural refinements. Comparing with values in the literature the min-

TABLE 1. ^{57}Fe Mössbauer parameters recorded from materials of composition $CaZrTi_{2-2x}Nb_xFe_xO_7$, showing the isomer shift (δ), quadrupolar splitting (Δ), and fraction of total spectrum

Compound	Component	δ ± 0.01 (mm/s)	Δ ± 0.01 (mm/s)	Area (%)
$CaZrTi_{1.6}Nb_{0.2}Fe_{0.2}O_7$	A	0.26	2.34	78
	B	0.33	0.81	22
$CaZrTi_{1.2}Nb_{0.4}Fe_{0.4}O_7$	A	0.26	2.35	73
	B	0.34	0.76	27
$CaZrTi_{0.8}Nb_{0.6}Fe_{0.6}O_7$	A	0.26	2.35	60
	B	0.34	0.74	40
$CaZrTi_{0.4}Nb_{0.8}Fe_{0.8}O_7$	A	0.26	2.39	49
	B	0.34	0.74	51
$CaZrNbFeO_7$	A	0.26	2.42	43
	B	0.35	0.78	57

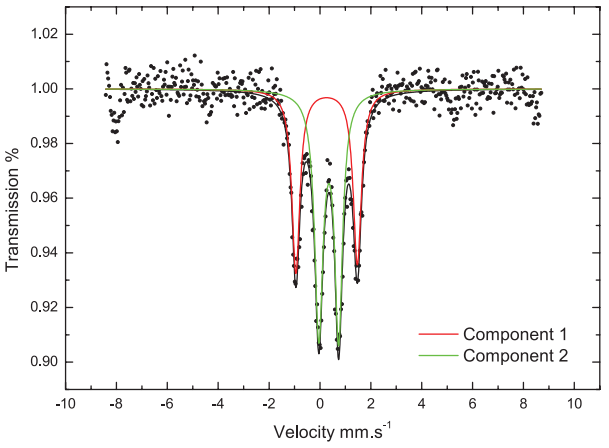

FIGURE 2. Representative Mossbauer spectrum from $CaZrTi_{1.2}Fe_{0.4}Nb_{0.4}O_7$ showing the two doublets indicative of a trigonal bipyramid and octahedron coordinated Fe^{3+} species.

eral sapphirine-2*M* was found to have Fe^{3+} located in similar geometries (Steffen et al. 1984). Within sapphirine-2*M*, the Fe^{3+} is located on two sites; the values recorded for these sites are shown in Table 2, and one of these sites approximates to those recorded here for the non-C2 site. Isomer shift and quadrupolar split parameters initially could not uniquely assign the second Fe^{3+} to a particular crystal site, it just confirmed octahedral co-ordination. For unique location the distortion for both octahedral sites were calculated and compared with those found in the sapphirine-2*M* model. The bond-angle distortions are calculated using the difference between each of the non-180° bonds and 90°, the bond-length variance is similar but uses the difference in bond-lengths compared to the average bond length (Lumpkin et al. 2008; Robinson et al. 1971).

The equations used are shown below and the values shown in Table 3;

$$\sigma_{ba}^2 = \sum_{i=1}^{n} \frac{(\theta_i - \theta_0)}{(n-1)} \quad (1)$$

$$\sigma_{bl} = \sum_{i=1}^{n} \frac{(d_i / d_0)^2}{n} \quad (2)$$

where σ_{ba} is the bond-angle variance; σ_{bl} the bond-length variance; θ_i the measured angle value; θ_0 the ideal angle; d_i is the average bond length from the center atom; d_0 the ideal bond length; and n the number of bonds being compared, i.e., 12 for angle and 6 for length variance

The bond-angle distortion is not significantly different to assign this second Fe^{3+} unambiguously, however, when the bond-length distortion is included it is possible to assign the Fe^{3+} to a specific site. Therefore the second Fe^{3+} has been assigned to the C1 cation position, i.e., the bond-length variance for C1 closely approximates that of the Fe1 site in sapphirine-2*M*. As can be seen in Table 1 the proportional area of the doublets change with increasing Fe^{3+} content, implying that one site is preferentially filled first, in this case the C2 site. Thus the Mössbauer data provides extra information about the location and proportion of the Fe^{3+} cations within the zirconolite-2*M* structure both aiding, and providing a secondary constraint to the structure refinements.

Rietveld refinements

As outlined earlier the refinement of the recorded data proceeded in two parts, the first part determined the unit-cell parameters, a function to describe the background and peak shapes using a Le Bail refinement. The wavelength of the lowest energy X-rays used was determined using a Le Bail refinement of NBS-640c Si powder. Once the refinements had converged these values were constrained and further refinements used the Rietveld method for determining atomic positions, isotropic thermal parameters, and site fractional occupancies. These refinements used the combination of high-resolution neutron powder and resonant X-ray diffraction data. The scattering parameters used in the refinements were the standard tabulated values within GSAS for the neutron diffraction data, and calculated using fprime for the X-ray data for those data that were not measured, i.e., Zr^{4+} and Nb^{5+}. In all refinements the disordered sites (C1, C2, and C3) were constrained such that x, y, z, and isothermal parameters were identical for each atom on each site with the overall composition fixed. Test refinements were undertaken using a constraint of identical isothermal parameters for C1, C2, and C3. However, these refinements became quickly unstable and led to unrealistic values.

Unit-cell parameters

The refined unit-cell parameters, shown in Table 4 and Figure 3, show a non-linear relationship with the replacement of $2Ti^{4+}$ by Fe^{3+}/Nb^{5+} within the HTB layers. The refined parameters obtained for $CaZrNbFeO_7$ are in broad agreement with those previously published by Belyaev et al. (1983) and Sinclair and Eggleton (1982), shown in Table 5.

$CaZrTi_2O_7$

The structural refinement of this end-member agrees broadly with those previously published with C2 located on a split position (Gatehouse et al. 1981) and is shown in Table 6 with the fit index parameters wR_p, R_p, and χ^2. Previous studies have

TABLE 2. The Mössbauer parameters for $CaZrTi_{1.2}Fe_{0.4}Nb_{0.4}O_7$ showing the comparable values for the second octahedrally coordinated Fe^{3+} site with that published for sapphirine-2*M*

System	Isomer shift (mm s^{-1})	Quadrupolar split (mm s^{-1})	Polyhedral co-ordination
$CaZrTi_{1.2}Fe_{0.4}Nb_{0.4}O_7$	0.26	2.35	5
	0.34	0.74	6
Sapphirine-2*M*	0.30	0.76	6

TABLE 3. Results from the asymmetry calculations for the octahedral sites in zirconolite-2*M* and sapphirine-2*M*

System	Site	Angular variance	Bond-length variance
$CaZrTi_{1.2}Fe_{0.4}Nb_{0.4}O_7$	C1	29.07	1.61
	C3	27.59	0.45
Sapphirine-2*M*	1	31.70	1.53
	2	28.02	2.55

Note: The upper/lower lines for each sample within the table refer to the different crystal sites within the structure.

indicated some disorder across the Ca and Zr sites (Gatehouse et al. 1981), these models were tested but found to give results that were statistically no more reliable than those presented here indicating that no disorder was observed in these samples.

$CaZrNbFeO_7$

Initially this end-member proved difficult to determine cation occupancy to values that were statistically significant. Three models were originally tried, based on previous results obtained using single wavelength X-rays, and Mössbauer spectroscopic data (Lumpkin et al. 2006). The three models are shown in Table 7, along with their final wR_p, R_p, and χ^2 fit index parameters. These models were based on the Mössbauer results that suggest that the Fe^{3+} occupies the C2 site preferentially, and when x = 1 the fractional occupancy is 0.5 (this site can only be occupied at 50%). The remaining Fe^{3+} and Nb^{5+} subsequently distributes

TABLE 4. Results obtained from combined refinements of unit-cell parameters, the values in brackets are the e.s.d. values calculated by GSAS, and are from the least-squares refinement of the data recorded

x	*a* (Å)	*b* (Å)	*c* (Å)	β (°)	*V* (Å³)
0	12.443024(11)	7.272901(7)	11.380867(11)	100.56430(10)	1012.4750(20)
0.1	12.455739(11)	7.276385(7)	11.387670(11)	100.56860(10)	1014.5870(20)
0.3	12.490726(16)	7.288121(9)	11.413671(15)	100.57590(10)	1021.3810(30)
0.5	12.527951(14)	7.304224(8)	11.426725(13)	100.60200(10)	1027.7750(10)
0.7	12.581563(8)	7.330757(8)	11.465700(8)	100.6427	1039.3180(20)
0.9	12.64620(9)	7.368726(11)	11.529889(18)	100.6419(10)	1055.965(4)
1	12.670281(12)	7.378349(7)	11.525772(11)	100.66950(10)	1058.8669(20)

TABLE 5. Published unit-cell values for Fe^{3+}- and Nb^{5+}-containing zirconolites (the data are from Coelho et al. 1997; Gatehouse et al. 1981)

Composition	*a* (Å)	*b* (Å)	*c* (Å)	β (°)	*V* (Å³)
$Ca_{0.87}Th_{0.13}ZrTi_{1.05}Fe_{0.455}Nb_{0.49}O_7$	12.431(1)	7.224(1)	11.483(3)	100.33(1)	1014.5(5)
$CaZrFeNbO_7$	12.74(2)	7.34(1)	11.49(2)	100.55(10)	1056.29

TABLE 6. Unit-cell structure obtained from combined refinement of $CaZrTi_2O_7$ using X-rays and neutrons

Name	Wyckoff site	x	y	z	U_{iso} *100	Frac
		wR_p 0.1063, R_p 0.1014, χ^2 2.76				
Ca	8*f*	0.37324(7)	0.12636(16)	0.49585(7)	0.447(20)	1.0
Zr	8*f*	0.12310(4)	0.12211(9)	0.97463(4)	2.187(13)	1.0
Ti1 (C1)	8*f*	0.24953(8)	0.12344(22)	0.74674(7)	0.346(17)	1.0
Ti2 (C2)	8*f*	0.46960(13)	0.05336(19)	0.25244(18)	0.27(4)	0.5
Ti3 (C3)	4*e*	0.0	0.12640(22)	0.25	0.302(27)	1.0
O1	8*f*	0.30569(11)	0.12679(29)	0.27877(12)	2.26(4)	1.0
O2	8*f*	0.47061(12)	0.13387(29)	0.10057(11)	1.54(4)	1.0
O3	8*f*	0.20838(14)	0.08524(22)	0.57122(14)	1.61(5)	1.0
O4	8*f*	0.39869(13)	0.16114(23)	0.72062(13)	1.74(5)	1.0
O5	8*f*	0.70759(13)	0.17321(22)	0.58342(14)	2.08(6)	1.0
O6	8*f*	0.00327(12)	0.12171(28)	0.41889(12)	1.72(4)	1.0
O7	8*f*	0.11190(15)	0.05400(19)	0.79053(15)	2.13(5)	1.0

Note: The wR_p, R_p, and χ^2 values are those reported by GSAS, U_{iso} is quoted in Å², for more information consult the GSAS/EXPGUI user manuals (Larson and Von Dreele 1994; Toby 2001).

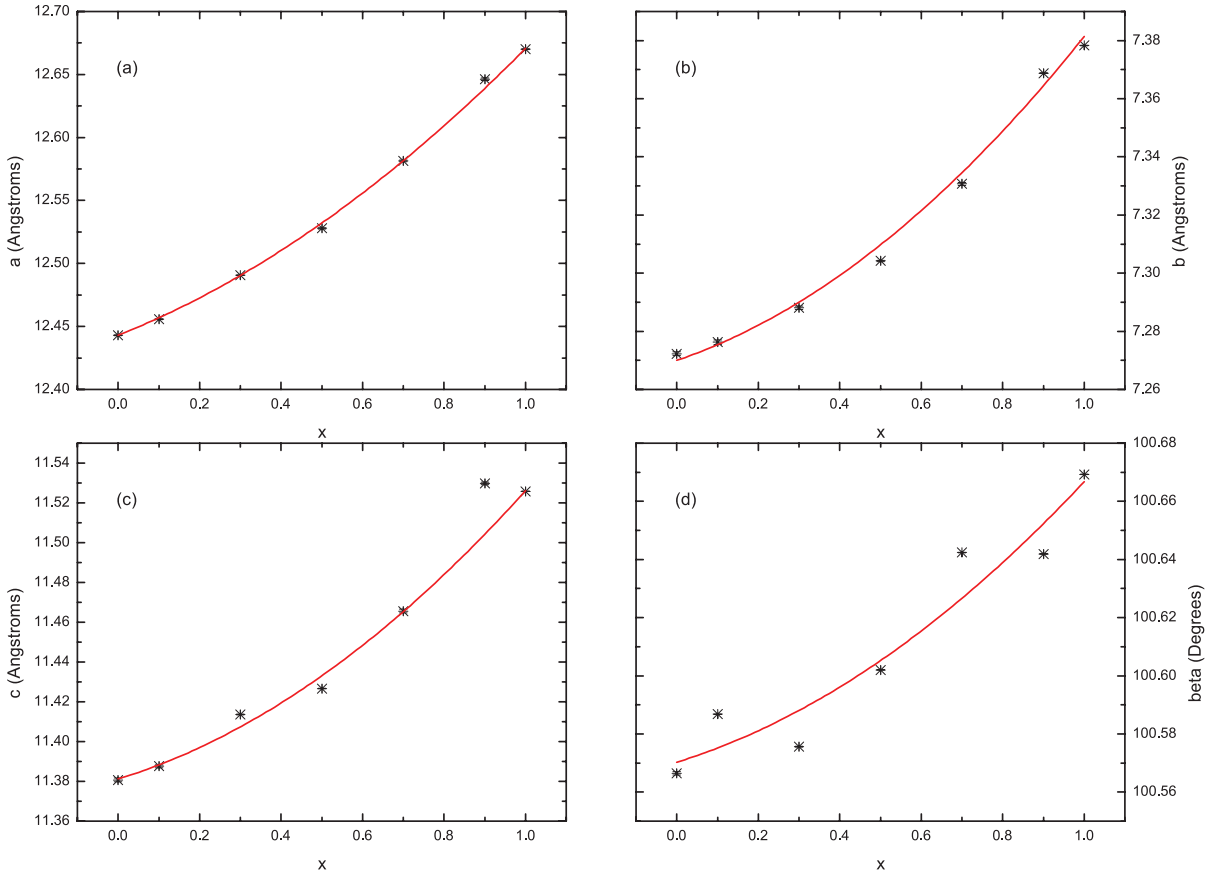

FIGURE 3. Four plots showing the non-linear changes in *a*, *b*, *c*, and the angle β with a curve fitted as a guide for the eye. The original data are provided in Table 4.

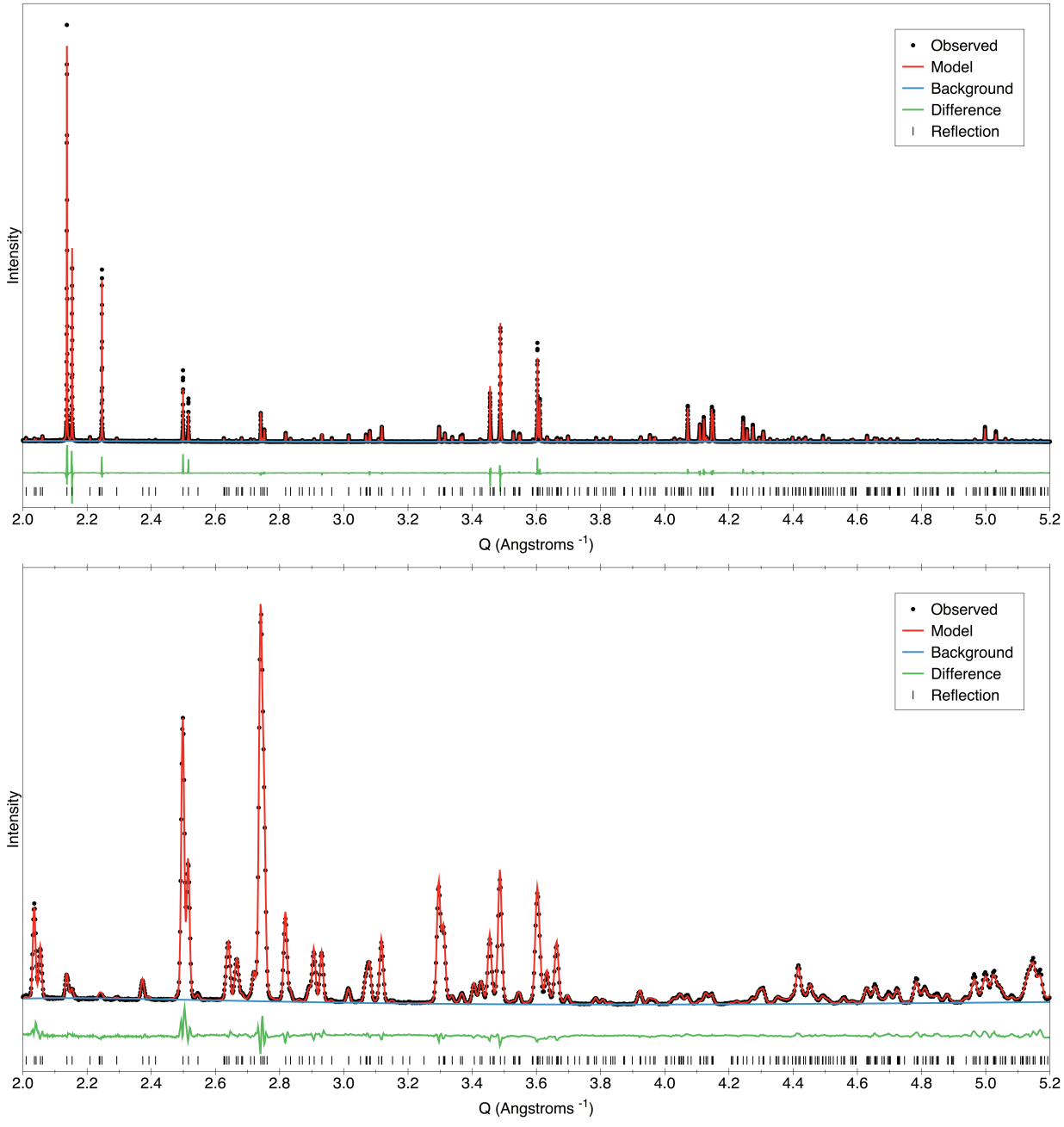

FIGURE 4. An example plot of the refined model for $CaZrTi_2O_7$ compared with recorded data for both neutron (**lower**) and X-ray diffraction data (**upper**). The recorded data are shown in black, the model is shown in red, and the difference is shown in green below. The data has been plotted in Q-space to allow a comparison of both fits, in reality the neutron data are time-of-flight, and the X-ray data are continuous wave angular data, which are not normally comparable.

across the C1 and C3 sites.

As can be seen from the refinements, there is very little statistical difference between model 1 and model 2. There is, however, a larger difference between these models and model 3, based on a model whereby the Fe^{3+} and Nb^{5+} occupancy was allowed to vary across both the C1 and C3 sites. Such a difference may describe the correct solution, however, this would disagree with the results obtained from Mössbauer spectroscopy, which indicates that Fe^{3+} prefers to occupy the C1 site. There are several possibilities for this difference but the most likely is the method of analysis used, i.e., least-squares minimization of model parameters vs. observed data. In the space group symmetry being used here, *C*2/*c*, there is only one fixed position during refinement, the C3 cation must reside on the special position (0, y, 0.25). All the other atoms are

free to move within the structure, within the limitations of the symmetry, and all atomic sites contribute to the intensity of each observed reflection. It is therefore possible, and probable, that refining the occupancy of the Fe^{3+} and Nb^{5+}, with the positional parameters for each constituent atom, gives rise to false minima being obtained, even with the absorption being accounted for. This is further complicated when the scattering parameters of Ca^{2+}, Zr^{4+}, Fe^{3+}, Nb^{5+}, and O^{2-} are compared, values shown in Table 8. The neutron scattering lengths for Zr^{4+} and Nb^{5+} are similar, while the X-ray scattering parameters for Fe^{3+} and Ca^{2+} are also similar, i.e., Z = 23 and 18, respectively. These small contrasts, even with increases from the use of resonant X-ray diffraction, make a clear structure difficult to obtain.

$CaZrTiFe_{0.5}Nb_{0.5}O_7$

To test the hypothesis that false minima had been observed for $CaZrNbFeO_7$, the diffraction patterns for $CaZrTiFe_{0.5}Nb_{0.5}O_7$ were analyzed. These refinements used the information provided by the Mössbauer spectra for the Fe^{3+} location as a guide, i.e., ~66% on C2. Refinements were undertaken whereby the amounts of Fe^{3+} across the C1 and C3 sites were changed and the effect on the refinements noted, example results from this analysis are shown in Table 9. The most likely model was one that placed the remaining Fe^{3+} on C1 with C3 occupied by Nb^{5+} and Ti^{4+}, the exact amounts obtained from a constrained refinement of site occupancies, shown in Table 10. The advantage of taking this approach stems from the extra information provided by the Ti^{4+}. Although Ti^{4+} and Ca^{2+} have identical electron numbers, i.e., 18, and would be expected to have similar X-ray scattering parameters, the negative neutron scattering length of Ti^{4+} provides extra contrast helping to avoid false minima when refining. To further restrain this fit the expected atomic charges were used to conserve an overall neutral charge.

$CaZrTi_{2-2x}Fe_xNb_xO_7$ – x = 0.1, 0.3, 0.7, and 0.9

Using the results from this $CaZrTiFe_{0.5}Nb_{0.5}O_7$, a model based on the following was used:

- C2 contains Fe^{3+} and Ti^{4+}, the amount of Fe^{3+} determined from the Mössbauer analysis.
- C1 contains the remaining Fe^{3+} and Ti^{4+}/Nb^{5+}.
- C3 contains Ti^{4+} and Nb^{5+} the exact amounts determined from a constrained co-refinement of fractional occupancies with the C1 site.

The occupancies from these refinements are shown in Table 11. The change in occupancy correlates with the general increase in Fe^{3+} and Nb^{5+} at the expense of Ti^{4+}, and does not show any large jumps or deviations. CIF[1] files are available on the web.

Bond-valence summations

Bond-valence summation provides a mechanism for checking a refinement and validity of a model. In some systems, it can help derive a model to fit the observed data. In this analysis, shown in Table 12, the standard values for R_0 for each of the cations were taken from Brese and O'Keefe (1991), and the average bond length for the polyhedra studied.

As can be seen in Table 12, the bond-valence summations broadly agree with expected values. There is a small deviation from "ideal" charge, e.g., Fe^{3+} should have a bond-valence summation of 3, however, in some samples it is found to be lower than "ideal." In all samples, the largest negative deficit, i.e., under bonded, occurs for the C2 (split site), where other sites are predominantly found to be over bonded. This deficit can be

TABLE 7. Unit-cell structures obtained from the three different models tested for $CaZrFeNbO_7$

Name	Wyckoff	x	y	z	U_{iso}*100	Frac Fe/Nb
Model 1: wR_p = 0.1249, R_p = 0.1111, χ^2 = 2.921						
Ca	8*f*	0.37677(8)	0.12347(19)	0.49708(8)	1.483(22)	1.00
Zr	8*f*	0.11926(4)	0.12832(8)	0.974373(34)	2.281(13)	1.00
C1	8*f*	0.24865(5)	0.12406(14)	0.74347(5)	0.715(12)	0.50/0.50
C2	8*f*	0.47087(11)	0.06952(15)	0.25151(15)	2.430(41)	0.50/0.00
C3	4*e*	0.000000	0.13108(16)	0.250000	2.371(20)	0.00/1.00
O1	8*f*	0.30165(13)	0.12702(30)	0.28512(14)	1.86(5)	1.00
O2	8*f*	0.46881(15)	0.13738(33)	0.09745(13)	1.78(5)	1.00
O3	8*f*	0.20436(16)	0.08169(23)	0.56876(15)	1.07(5)	1.00
O4	8*f*	0.39578(15)	0.16061(27)	0.71542(15)	1.76(5)	1.00
O5	8*f*	0.71143(16)	0.17661(24)	0.58436(16)	1.96(6)	1.00
O6	8*f*	–0.00434(14)	0.11928(29)	0.42021(14)	1.72(5)	1.00
O7	8*f*	0.11282(18)	0.05607(24)	0.79397(17)	1.87(6)	1.00
Model 2: wR_p = 0.1254, R_p = 0.1114, χ^2 = 2.946						
Ca	8*f*	0.37635(8)	0.12246(18)	0.49596(8)	1.700(21)	1.00
Zr	8*f*	0.11908(4)	0.12845(8)	0.974884(34)	2.392(12)	1.00
C1	8*f*	0.24863(5)	0.12375(13)	0.74284(5)	1.296(12)	0.00/1.00
C2	8*f*	0.46956(10)	0.06860(15)	0.25137(15)	2.149(4)	0.50/0.00
C3	4*e*	0.000000	0.13058(16)	0.250000	0.598(19)	1.00/0.00
O1	8*f*	0.30168(12)	0.12885(29)	0.28364(14)	1.36(5)	1.00
O2	8*f*	0.46909(14)	0.14037(33)	0.09745(13)	1.54(5)	1.00
O3	8*f*	0.20563(16)	0.08250(25)	0.56867(15)	1.49(6)	1.00
O4	8*f*	0.39660(15)	0.16677(27)	0.71722(15)	1.53(5)	1.00
O5	8*f*	0.70941(16)	0.18171(23)	0.58284(16)	1.35(6)	1.00
O6	8*f*	–0.00607(14)	0.12100(29)	0.41584(14)	1.36(5)	1.00
O7	8*f*	0.10921(17)	0.05150(25)	0.79405(18)	1.89(6)	1.00
Model 3: wR_p = 0.1208, R_p = 0.1082, χ^2 = 2.735						
Ca	8*f*	0.37665(8)	0.12293(18)	0.49666(7)	1.77(20)	1.00
Zr	8*f*	0.11915(4)	0.12839(8)	0.974528(32)	2.58(10)	1.00
C1	8*f*	0.24856(5)	0.12356(13)	0.74309(4)	0.92(12)	0.21/0.79
C2	8*f*	0.46946(10)	0.06708(15)	0.25155(15)	2.39(4)	0.50/0.00
C3	4*e*	0.000000	0.13079(15)	0.250000	1.25(18)	0.58/0.42
O1	8*f*	0.30083(12)	0.12864(29)	0.28376(14)	1.78(5)	1.00
O2	8*f*	0.46886(14)	0.13961(32)	0.09774(13)	1.67(5)	1.00
O3	8*f*	0.20485(15)	0.08221(23)	0.56824(15)	1.25(5)	1.00
O4	8*f*	0.39554(15)	0.16499(26)	0.71682(14)	1.46(5)	1.00
O5	8*f*	0.71011(15)	0.18073(22)	0.58384(15)	1.53(6)	1.00
O6	8*f*	–0.00603(14)	0.12121(28)	0.41724(13)	1.45(4)	1.00
O7	8*f*	0.11093(17)	0.05351(23)	0.79435(17)	1.85(6)	1.00

Note: The *wRp*, *Rp*, and χ^2 values are those reported by GSAS, U_{iso} is quoted in Å^2, for more information consult the GSAS/EXPGUI user manuals (Larson and Von Dreele 1994; Toby 2001).

TABLE 8. Standard coherent neutron scattering lengths (Sears 1992) and electron numbers for the atomic species used in this study

Element	Scattering length (fm)	Electron number
Ca^{2+}	4.7	18
Ti^{4+}	–3.438	18
Fe^{3+}	9.45	23
Zr^{4+}	7.16	36
Nb^{5+}	7.054	36
O^{2-}	5.803	10

[1] Deposit item AM-12-012, CIFs. Deposit items are available two ways: For a paper copy contact the Business Office of the Mineralogical Society of America (see inside front cover of recent issue) for price information. For an electronic copy visit the MSA web site at http://www.minsocam.org, go to the *American Mineralogist* Contents, find the table of contents for the specific volume/issue wanted, and then click on the deposit link there.

TABLE 9. Example models and fractional occupancies tested, with the recorded χ^2

Model	C1 Nb/Fe/Ti	C2 Nb/Fe/Ti	C3 Nb/Fe/Ti	χ^2
1	0.0/0.17/0.83	0/0.33/0.17	1.0/0.0/0.0	5.21
2	0.17/0.07/0.76	0/0.33/0.17	0.66/0.2/0.14	4.30
3	0.1/0.17/0.73	0.07/0.33/0.1	0.66/0.0/0.34	3.85
4	0.17/0.17/0.66	0.0/0.33/0.17	0.66/0.0/0.34	3.74

TABLE 10. Unit-cell positions for $CaZrTiFe_{0.5}Nb_{0.5}O_7$ (for *a, b, c,* and ß see Table 5)

Name	Wyckoff site	x	y	z	U_{iso}*100	Frac (Ti/Fe/Nb)
			wR_p 0.1098, R_p 0.1014, χ^2 2.523			
Ca	8*f*	0.37500(5)	0.12327(11)	0.49615(5)	0.885(13)	1.00
Zr	8*f*	0.120624(25)	0.12688(5)	0.972939(23)	1.558(7)	1.00
C1	8*f*	0.24985(4)	0.12456(10)	0.74455(4)	1.216(10)	0.47/0.17/0.36
C2	8*f*	0.47068(7)	0.05956(11)	0.25189(10)	0.799(23)	0.17/0.33/0
C3	4*e*	0.0	0.12743(13)	0.25	1.454(16)	0.73/0/0.27
O1	8*f*	0.30127(8)	0.13051(19)	0.28278(9)	2.033(31)	1.00
O2	8*f*	0.46962(9)	0.13773(19)	0.09720(8)	1.1151(28)	1.00
O3	8*f*	0.20534(10)	0.08372(14)	0.57080(9)	0.808(32)	1.00
O4	8*f*	0.39595(9)	0.16728(15)	0.71794(9)	1.232(32)	1.00
O5	8*f*	0.71063(9)	0.17600(15)	0.58300(10)	1.167(35)	1.00
O6	8*f*	–0.00320(9)	0.12173(18)	0.41761(8)	1.1079(28)	1.00
O7	8*f*	0.11246(10)	0.05264(13)	0.79133(10)	1.009(31)	1.00

Notes: The wR_p, R_p, and χ^2 values are those reported by GSAS, U_{iso} is quoted in Å^2. The values in brackets are the e.s.d. values provided by GSAS, for more information consult the GSAS/EXPGUI user manuals (Larson and Von Dreele 1994; Toby 2001).

TABLE 11. Fractional occupancies of sites C1, C2, and C3

System	C1 Ti/Fe/Nb	C2 Ti/Fe/Nb	C3 Ti/Fe/Nb
$CaZrTi_2O_7$	1/0/0	0.5/0/0	1/0/0
$CaZrTi_{1.8}Nb_{0.1}Fe_{0.1}O_7$	0.9/0.02/0.08	0.42/0.08/0	0.96/0/0.04
$CaZrTi_{1.4}Nb_{0.3}Fe_{0.3}O_7$	0.7/0.08/0.22	0.28/0.22/0	0.86/0/0.14
$CaZrTiNb_{0.5}Fe_{0.5}O_7$	0.47/0.17/0.36	0.17/0.33/0	0.73/0/0.27
$CaZrTi_{0.6}Nb_{0.7}Fe_{0.7}O_7$	0.24/0.32/0.44	0.12/0.38/0	0.48/0/0.52
$CaZrTi_{0.1}Nb_{0.9}Fe_{0.9}O_7$	0.07/0.48/0.45	0.08/0.42/0	0.11/0/0.89
$CaZrNbFeO_7$	0/0.5/0.5	0/0.5/0	0/0/1

Notes: Values are reduced to 2 decimal places, full values are provided in the accompanying information[1]. Occupancies obtained from refinement of fractional occupancies are based on constraints from the ^{57}Fe Mössbauer spectroscopic results.

TABLE 12. Calculated bond valence summations based on occupancies and bond lengths from refined structures, values in parentheses are errors in the last digit

x	Ca-O	Zr-O	C1-O	C2-O	C3-O
0	2.144(10)	3.742(16)	4.123(21)	3.745(21)	4.308(19)
0.1	2.135(9)	3.753(14)	4.188(20)	3.507(20)	4.388(18)
0.3	2.138(8)	3.725(13)	4.308(17)	3.066(14)	4.407(15)
0.5	2.106(8)	3.694(14)	4.369(18)	2.833(12)	4.599(19)
0.7	2.063(8)	3.703(13)	4.206(16)	2.703(11)	4.708(17)
0.9	2.053(12)	3.586(19)	3.953(23)	2.683(17)	4.917(26)
1	1.994(12)	3.742(21)	4.009(23)	2.636(16)	4.811(26)

Notes: The calculations have been made using a weighted average bond length for R_0 based on the occupancies for C1, C2, and C3 found in Table 11.

minimized if all the oxygen surrounding the C2 site are used including those further than the expected bond lengths, for example in $CaZrNbFeO_7$ the summation increases from 2.78 to 2.88. It is highly likely that this is due to the nature of the structure, and can be explained thus.

If the HTB layers within zirconolite are taken as a single entity, they can be described using two apex-sharing octahedra (C1 and C3), forming a structure of three and six member rings, shown in Figure 1. Within the six member rings, the C2 cation is located, in a site that can only be 50% occupied. This position provides a large degree of positional freedom but does not have any effect on the size of the void; this is determined by the polyhedra linkage formed by C1 and C3. It is therefore quite possible for this cation site to be "under" bonded formally, as it is essentially a non-structure determining cation, while still being a valid refinement, the extra charge being distributed within the coordination volume. A potential secondary explanation in systems that contain Fe^{3+} is a slight reduction of Fe^{3+} to Fe^{2+}, there was no experimental evidence for this, it would have been expected to be seen in the Mössbauer spectra, but in this system it would be difficult to observe and cannot be entirely discounted.

DISCUSSION

As can be seen in the collected results the system $CaZrTi_{2-2x}Fe_xNb_xO_7$ is not simple and highly complex to refine. Unlike pyrochlore, a close relative, it is not possible to uniquely assign diffraction reflections to particular atomic sites, in this space group all atoms contribute to all reflection intensities. A further complication is that only the C3 site, has a positional restraint within the unit cell, i.e., the 4*e* Wyckoff site (0, y, 1/4) and can only move along the y-axis. All other locations are general positions and able to move in three dimensions during the refinement while following symmetry constraints (glide, twofold rotation, and centrosymmetry). Since there are 11 atomic sites with general positions and 1 atomic site on the 4*e* special position, giving rise to a total of 92 atoms, any refinement of such a structure will be complex. To obtain a model structure that is as correct as possible, the extra information provided by the Mössbauer spectra collected using ^{57}Fe, and the extra contrast provided by the neutron diffraction and the resonant X-ray diffraction was vital. If this extra information was not present then false minima refinements were possible, and highly likely.

The results indicate that as Fe^{3+}/Nb^{5+} is co-doped for Ti^{4+}, the following occurs (shown in Table 11):

• Initially the Fe^{3+} preferentially locates onto the split C2 site (3:1 vs. the C1 site), and occupies this position with the balance completed by Ti^{4+}. As the concentration of Fe^{3+} increases both this site and the C1 increase in Fe^{3+} concentration, but C1 increases at a quicker rate, till at ca. $CaZrTi_{0.4}Fe_{0.8}Nb_{0.8}O_7$ both sites have similar fractions of Fe^{3+}. After this point the C1 continues to increase in Fe^{3+} content more rapidly than C2.

• The Nb^{5+} follows a similar trend, but with one small difference, here it preferentially occupies the C1 site until $CaZrTi_{0.6}Fe_{0.7}Nb_{0.7}O_7$, after this sample C3 fills more rapidly until complete occupancy occurs.

There are many possibilities for these preferential occupancies, one likely explanation correlates with the ionic radii of Fe^{3+}, Ti^{4+}, and Nb^{5+}. If the Shannon ionic radii (Shannon 1976; Shannon and Prewitt 1969, 1970) are compared, there is little difference between Nb^{5+} and Fe^{3+} when tetrahedrally coordinated by oxygen. However, there is a large difference when octahedrally coordinated. Therefore it is highly likely that Nb^{5+} will prefer octahedrally coordinated environments, such as C1 and C3 than effectively tetrahedral environments, i.e., C2.

Previous studies of Nb containing bismuth based zirconolites by Levin et al. (2002a, 2002b) have also located the Nb^{5+} on both the C1 and C3 sites. A naturally occurring zirkelite (Gatehouse

et al. 1981) (radiation-damaged zirconolite) located Fe^{3+} on the C1 and C2 sites, and Nb^{5+} on C1 and C3, thus agreeing with the data presented here.

During the refinement process structures based on the non-centrosymmetric *Cc* space group were tested as a confirmation of correct symmetry. Although the wR_p and R_p values decreased, the number of variables (atomic position, occupancy, thermal parameters) effectively doubled, due to the loss of centrosymmetry, i.e., the loss of the constraint (x, y, z) moving in an identical manner to (1 – x, 1 – y, 1 – z). This increased the complexity of the refinement, providing more degrees of freedom to increase the reliability of fit, i.e., an atom on (x, y, z) can be move independently of an atom formerly on (1 – x, 1 – y, 1 – z). Since increasing degrees of freedom generally results in better fits, even when wrong, *Cc* symmetry was not proven.

Finally an explanation for the relatively large wR_p and R_p fit indices should be provided. Due to the exceptionally high resolution available for ID31, and low-instrumental component to the peak shape, the peaks are very narrow. To refine such narrow peaks adequately a small angular step size was used, this subsequently provided a large number of points between reflections, which have a low-noise component, thus increasing the values obtained for fit indices. If a graphical difference is plotted, as shown in Figure 4 for $CaZrTi_2O_7$, the refinements are not poor; it is purely the low-background and low-statistical noise that increases the fit indices.

Acknowledgments

The authors wish to acknowledge the funding provided by the EPSRC for experiment time at HRPD, ISIS, and the ESRF for providing the time at ID31, ESRF. The authors acknowledge the help of Gordon Oates for collection of the Mössbauer data.

References cited

Belyaev, I., Aver'yanova, L.N., and Lopatin, S.S. (1983) Quarternary oxides CaABB'O with zirconolite crystal structure. Zhurnal Neorganicheskoi Khimii, 28, 915–918.

Berry, F., Marco, J., Ponton, C., and Whittle, K.R. (2001) Preparation and characterization of rare earth-doped strontium hexaferrites $Sr_{1-x}M_xFe_{12}O_{19}$(M = La, Eu). Journal of Materials Science Letters, 20, p. 431–434.

Berry, F.J., Lumpkin, G.R., Oates, G., and Whittle, K.R. (2005) Iron-57 Mossbauer spectroscopy study of phases in the $CaZrTi_{2-2x}Nb_xFe_xO_7$ zirconolite system. Hyperfine Interactions, 166, p. 363–366.

Brese, N. and O'Keeffe, M. (1991) Bond-valence parameters for solids. Acta Crystallographica, B47 192–197.

Coelho, A.A., Cheary, R., and Smith, K.L. (1997) Analysis and structural determination of Nd-substituted zirconolite-4*M*. Journal of Solid State Chemistry, 129, 346–359.

Ewing, R.C. (2007) Ceramic matrices for plutonium disposition. Progress in Nuclear Energy, 49, 635–643.

Fitch, A.N. (2004) The high resolution powder diffraction beam line at ESRF. Journal of Research of the National Institute of Standards and Technology, 109, 133–142.

Gatehouse, B., Grey, I., Hill, R., and Rossell, H. (1981) Zirconolite, $CaZr_xTi_{3-x}O_7$; structure refinements for near-end-member compositions with x = 0.85 and 1.30. Acta Crystallographica, B37, 306–312.

Grey, I., Mumme, W., Ness, T., Roth, R., and Smith, K.L. (2003) Structural relations between weberite and zirconolite polytypes—refinements of doped 3*T* and 4*M* $Ca_2Ta_2O_7$ and 3*T* $CaZrTi_2O_7$. Journal of Solid State Chemistry, 174, 285–295.

Ibberson, R.M., David, W.I.F., and Knight, K.S. (1992) Rutherford Appleton Laboratory Report, RAL92-031.

Larson, A. and Von Dreele, R. (1994) General Structure Analysis System (GSAS). Los Alamos National Laboratory Report LAUR 86-748.

Le Bail, A., Duroy, H., and Fourquet, J. (1988) Ab-initio structure determination of $LiSbWO_6$ by X-ray powder diffraction. Materials Research Bulletin, 23, 447–452.

Levin, I., Amos, T., Nino, J., Vanderah, T., Randall, C.A., and Lanagan, M. (2002a) Structural study of an unusual cubic pyrochlore $Bi_{1.5}Zn_{0.92}Nb_{1.5}O_{6.92}$. Journal of Solid State Chemistry, 168, 69–75.

Levin, I., Amos, T.G., Nino, J.C., Vanderah, T.A., Reaney, I., Randall, C.A., and Lanagan, M.T. (2002b) Crystal structure of the compound $Bi_2Zn_{2/3}Nb_{4/3}O_7$. Journal of Materials Research, 17, 1406.

Lumpkin, G.R. (2001) Alpha-decay damage and aqueous durability of actinide host phases in natural systems. Journal of Nuclear Materials, 289, 136–166.

Lumpkin, G., Whittle, K., Howard, C., Zhang, Z., Berry, F., Oates, G., Williams, C., and Zaitsev, A. (2006) Crystal chemistry and cation ordering in zirconolite 2*M*. Scientific Basis for Nuclear Waste Management XXIX, 932, 639–645.

Lumpkin, G.R., Smith, K.L., Blackford, M., Thomas, B.S., and Whittle, K.R. (2008) Experimental and atomistic modeling study of ion irradiation damage in thin crystals of the TiO_2 polymorphs. Physical Review B, 77, 214201.

Robinson, K., Gibbs, G., and Ribbe, P. (1971) Quadratic elongation: A quantitative measure of distortion in coordination polyhedra. Science, 172, 567–570.

Sears, V.F. (1992) Neutron scattering lengths and cross sections. Neutron News, 3, 26–37.

Shannon, R. (1976) Revised effective ionic radii and systematic studies of interatomic distances in halides and chalcogenides. Acta Crystallographica, A32, 751–767.

Shannon, R. and Prewitt, C. (1969) Effective ionic radii in oxides and fluorides. Acta Crystallographica, B25, 925–946.

——— (1970) Revised values of effective ionic radii. Acta Crystallographica, B26, 1046–1048.

Sinclair, W. and Eggleton, R. (1982) Structure refinement of zirkelite from Kaiserstuhl, West Germany. American Mineralogist, 67, 615–620.

Steffen, G., Seifert, F., and Amthauer, G. (1984) Ferric iron in sapphirine; a Moessbauer spectroscopic study. American Mineralogist, 69, 339–348.

Toby, B. (2001) EXPGUI, a graphical user interface for GSAS. Journal of Applied Crystallography, 34, 210–213.

Yudintsev, S.V. (2003) A structural-chemical approach to selecting crystalline matrices for actinide immobilization. Geology of Ore Deposits, 45, 151–165.

Manuscript received March 29, 2011
Manuscript accepted October 13, 2011
Manuscript handled by Simon Redfern